

pubs.acs.org/JPCA Article

# Charge Transfer and Spin Dynamics in a Zinc Porphyrin Donor Covalently Linked to One or Two Naphthalenediimide Acceptors

Laura Bancroft, Jinyuan Zhang, Samantha M. Harvey, Matthew D. Krzyaniak, Peng Zhang, Richard D. Schaller, David N. Beratan,\* Ryan M. Young,\* and Michael R. Wasielewski\*



Cite This: J. Phys. Chem. A 2021, 125, 825-834



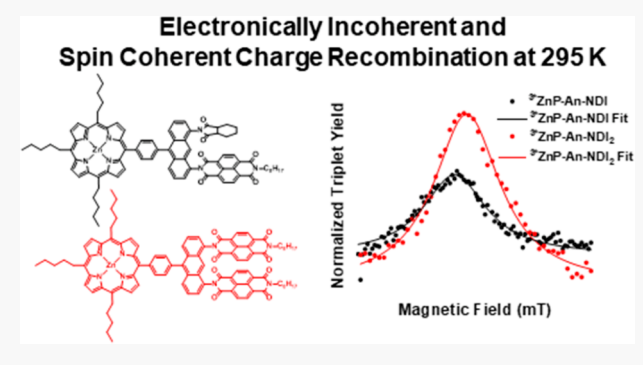
ACCESS

Metrics & More

Article Recommendations

Supporting Information

ABSTRACT: Quantum coherence effects on charge transfer and spin dynamics in a system having two degenerate electron acceptors are studied using a zinc 5,10,15-tri(n-pentyl)-20-phenylporphyrin (ZnP) electron donor covalently linked to either one or two naphthalene-1,8:4,5-bis(dicarboximide) (NDI) electron acceptors using an anthracene (An) spacer, ZnP-An-NDI (1) and ZnP-An-NDI<sub>2</sub> (2), respectively. Following photoexcitation of 1 and 2 in toluene at 295 K, femtosecond transient absorption spectroscopy shows that the electron transfer (ET) rate constant for 2 is about three times larger than that of 1, which can be accounted for by the statistical nature of incoherent ET as well as the electron couplings for the charge separation reactions. In contrast, the rate constant for



charge recombination (CR) of 1 is about 25% faster than that of 2. Using femtosecond transient infrared spectroscopy and theoretical analysis, we find that the electron on  $NDI_2^{\bullet-}$  in 2 localizes onto one of the two NDIs prior to CR, thus precluding electronically coherent CR from  $NDI_2^{\bullet-}$ . Conversely, CR in both 1 and 2 is spin coherent as indicated by the observation of a resonance in the <sup>3\*</sup>ZnP yield following CR as a function of applied magnetic field, giving spin—spin exchange interaction energies of 2J = 210 and 236 mT, respectively, where the line width of the resonance for 2 is greater than 1. These data show that while CR is a spin-coherent process, incoherent hopping of the electron between the two NDIs in 2, consistent with the lack of delocalization noted above, results in greater spin decoherence in 2 relative to 1.

# **■ INTRODUCTION**

Expanding simple electron donor—acceptor (D—A) systems to larger structures with multiple donors and/or acceptors raises the possibility that site-to-site charge (spin) hopping or complete delocalization, where the wave function simultaneously involves two or more sites, can influence both charge transfer and spin dynamics. Previously, systems with either two identical donors or acceptors have been studied using noncovalent D/A mixtures<sup>1–3</sup> and assemblies,<sup>4</sup> as well as covalent D—A dyads<sup>5</sup> and triads,<sup>6,7</sup> all of which have the potential for electron/hole hopping or delocalization between the two A or D species, respectively.<sup>8,9</sup>

In the specific case of two degenerate electron acceptors, D-A<sub>2</sub>, we have shown that electron transfer can proceed coherently to a delocalized state of the dimeric acceptor. The charge transfer is a consequence of renormalization of the electronic coupling for electron transfer as well as the system bath interactions. <sup>10</sup> Under cryogenic conditions, delocalization is maintained throughout the charge separation process, resulting in a nonstatistical rate enhancement for charge transfer to two acceptors relative to one acceptor. We demonstrated this fully coherent charge transfer in a triptycene-bridged anthracene-benzoquinone system, where

electron transfer from the anthracene lowest excited singlet state to two equivalent benzoquinones occurs five times faster than to a single benzoquinone acceptor. Similarly, using a p-(9-anthryl)-N,N-dimethylaniline (DMA-An) donor and a dimeric naphthalene-1,8:4,5-bis(dicarboximide) (NDI) acceptor, we observed a smaller nonstatistical rate enhancement factor of  $2.6 \pm 0.2$  for charge separation, and also a factor of  $2.0 \pm 0.2$  for charge recombination. <sup>11</sup>

Coherent electron spin dynamics also play an important role in D–A systems intrinsic to natural <sup>12,13</sup> and artificial <sup>14,15</sup> photosynthesis, avian navigation, <sup>16,17</sup> and quantum information science (QIS). <sup>18–22</sup> In the context of natural and artificial photosynthesis, the polarization and delocalization of spin among multiple cofactors plays a crucial role in dictating the reaction mechanism and kinetics. <sup>23,24</sup> With regard to QIS, photogenerated radical pairs in organic D–A molecules have

Received: November 20, 2020 Revised: January 8, 2021 Published: January 15, 2021





many desirable qualities that make them promising spin qubit pairs (SQPs) and that fulfill the well-known DiVincenzo criteria for viable qubits. For example, subnanosecond electron transfer from D to A following laser photoexcitation produces an entangled SQP having a well-defined spin state, which allows for reliable execution of quantum gate operations without the use of ultralow temperatures or high magnetic fields. 12,22

Spin hopping or delocalization can have a significant impact on SQP spin coherence. For example, we recently compared the spin dynamics of a covalent  $D^{\bullet +}-C-A_2^{\bullet -}$  triad system to the corresponding  $D^{\bullet +}-C-A^{\bullet -}$  system, where C is a light-absorbing chromophoric acceptor. Photogeneration of the SQP in a magnetic field,  $B_0$ , results in Zeeman splitting of the SQP triplet sublevels (Figure 1), where the spin–spin

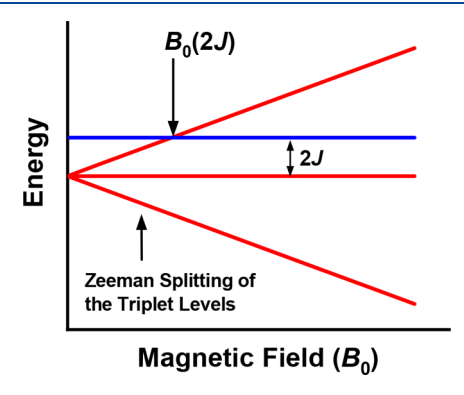


**Figure 1.** Zeeman splitting of RP energy levels (2J > 0).

exchange coupling, 2J, is the energy gap between the singlet and triplet SQP states. This coupling is primarily a throughbond interaction, while the corresponding spin—spin dipolar interaction, D, is a through-space interaction. When  $B_0\gg 2J$  and D, the  $|T_{+1}\rangle$ ,  $|T_0\rangle$ , and  $|T_{-1}\rangle$  eigenstates are quantized along  $B_0$  and the  $|S\rangle$  and  $|T_0\rangle$  state energies remain field invariant. Under these conditions, mixing between the initially populated  $|S\rangle$  and unpopulated  $|T_0\rangle$  states of the SQP results in zero quantum coherence between  $|S\rangle$  and  $|T_0\rangle$ . The value of 2J is <5 mT in  $D^{\bullet+}-C-A^{\bullet-}$  and  $D^{\bullet+}-C-A^{\bullet-}_2$  because there are a large number of bonds separating the two radicals in these triads. In addition, the value of D is also less than 0.2 mT because of the long distance between the two spins. Our earlier work showed that rapid electron hopping within the dimeric acceptor of  $D^{\bullet+}-C-A_2^{\bullet-}$  results in faster decoherence of the mixed  $|S\rangle$  and  $|T_0\rangle$  states than in the single acceptor

 $D^{\bullet+}-C-A^{\bullet-}$  reference system.<sup>7</sup> This work also showed magnetic field dependent changes in the SQP population since 2J is comparable to both the differential hyperfine interactions and the relaxation effects between  $D^{\bullet+}-C-A^{\bullet-}$  and  $D^{\bullet+}-C-A^{\bullet-}$ . In contrast, if 2J is large, coherent spin evolution is generally inhibited when  $B_0=0$  and the system can remain locked in the initially populated |S| state for long times.<sup>39</sup> However, applying a magnetic field  $B_0=2J$  turns on  $|S| \leftrightarrow |T_{-1}|$  (2J > 0) or  $|S| \leftrightarrow |T_{-1}|$  (2J < 0) spin mixing, which allows one to probe the spin dynamics of the system.

To explore charge transfer and spin coherence in a system where 2I is much larger than the hyperfine interactions, recombination is slow, and a local triplet state is energetically favorable, we designed a covalent D-A<sub>2</sub> molecule comprising a zinc 5,10,15-tri(*n*-pentyl)-20-phenylporphyrin (ZnP) chromophoric electron donor and one or two NDI electron acceptors linked by an anthracene (An) spacer, ZnP-An-NDI (1) and ZnP-An-NDI<sub>2</sub> (2), respectively (Figure 2). Compound 2 has two  $\pi$ -stacked NDI acceptors, while 1 has a photo- and electrochemically innocent 1,2-cyclohexanedicarboximide in place of the second NDI acceptor. The An spacer places the two NDI acceptors of 2 in a  $\pi$ -stacked geometry, <sup>40</sup> which has been shown previously to result in significant electronic coupling between them. <sup>41</sup> The combination of the ZnP donor and NDI acceptor(s) yields a large free energy of reaction for charge separation and the An spacer places the SQP sufficiently close to ensure large 2J values. 42,43 The energy of the ZnP triplet state is 1.6 eV,44 which opens a triplet charge recombination pathway and enables the direct measurement of 2J using magnetic field-resolved transient absorption spectroscopy. The measured 2J values, in combination with transient infrared absorption measurements and theoretical analysis, allow us to assess the influence of quantum coherence on the charge recombination and spin dynamics of the SQP in

# METHODS

**Steady-State Spectroscopy.** UV–visible absorption spectra were obtained using a Shimadzu UV-1800 spectrometer in a quartz cuvette with a 1 mm path length.

**Transient Absorption Spectroscopy.** Femtosecond transient absorption experiments were performed using the instruments described in previous accounts. The 560 nm, ∼100 fs pump pulse was generated using a commercial collinear optical parametric amplifier (TOPAS-Prime, Light-Conversion, LLC) while the 414 nm pump was the second harmonic of the fundamental. The pump pulse was depolarized

Figure 2. Chemical structures of molecules studied.

to suppress polarization-dependent dynamics in the signal. The pump pulses had energies of 1 µJ/pulse. Spectra were collected using a customized Helios/EOS spectrometer (Ultrafast Systems, LLC). All transient absorption data sets were collected on samples with a path length of 1 mm and an optical density of ~0.5 at 414 nm for the toluene data and  $\sim$ 0.25 at 560 nm for the 1,4-dioxane- $d_8$  data. All samples were put through three freeze-pump-thaw cycles to remove oxygen. Solution samples were stirred during run time to avoid degradation from localized heating. All data sets were background-subtracted to remove scatter from the pump pulse and corrected for time zero offsets and group delay dispersion using Surface Xplorer (Ultrafast Systems, LLC). The data sets were then each subjected to a global wavelength fitting analysis using a sequential 2-step model: A -> B -> C for the femtosecond transient absorption data and  $B \to C \to G$  for the nanosecond transient absorption data. For fitting the femtosecond transient absorption data, the rate constant  $k_{\rm BC}$  was fixed at the value obtained from the nanosecond transient absorption data fit. The kinetic traces were fit at five to six wavelengths across the relevant spectral features of the species formed in each of the experiments.

Transient Femtosecond Infrared Spectroscopy. The femtosecond time-resolved infrared (fs IR) absorption apparatus has also been described previously, and it was equipped with a Helios-FIRE IR spectrometer (Ultrafast Systems, LLC). The 560 nm excitation pulses were attenuated to 2  $\mu$ J/pulse and depolarized. The time resolution was ~500 fs. Difference spectra were obtained by modulating the pump at 500 Hz using the optical chopper in the Helios-IR spectrometer. Spectra were acquired in 1000 nm windows spanning 5600-8200 nm (1219-1785 cm<sup>-1</sup>) and combined without scaling prior to kinetic analysis. The fs IR spectra were calibrated using the ground state FTIR spectra. The samples were prepared in 1,4-dioxane- $d_8$  with an optical density of ~0.125 at 560 nm in a demountable cell (Harrick Scientific) with a 500  $\mu$ m Teflon spacer with 2 mm CaF<sub>2</sub> windows. The sample holder was rastered during experiments to reduce the effects of local heating. Both data sets were backgroundsubtracted to remove pump pulse scatter and corrected for time zero offsets and group delay dispersion using Surface Xplorer (Ultrafast Systems, LLC). The data sets were then each subjected to a global wavelength fitting analysis using a sequential 2-step model:  $A \rightarrow B \rightarrow C$ . The kinetic traces were fit at five wavelengths across the relevant spectral features of the species observed in each of the experiments.

**Magnetic Field Effects.** NsTA experiments were performed to monitor the charge recombination triplet yield of  $^{3}*\mathrm{ZnP}$  as a function of applied magnetic field using an instrument described previously. A 414 nm excitation pump pulse was used to excite the Soret band of the ZnP subunit. The optical density of the samples was  $\sim\!0.5$  with a 1 mm path length at 414 nm. The nsTA spectra were integrated over 450–500 nm and 0.5–10  $\mu\mathrm{s}$  at each magnetic field value to ensure that only  $^{3}*\mathrm{ZnP}$  was monitored. Periodically, the magnetic field was brought back to 0 mT to monitor the baseline and the  $^{3}*\mathrm{ZnP}$  yields were then normalized to the yield at zero magnetic field.

**Computational Details.** Molecular structures of the ground and excited state species were optimized using density functional theory (DFT) and time-dependent density functional theory (TDDFT) with the phe0 functional and the madef2-SVP basis set. The solvent effects were included using

the PCM model (for toluene). The empirical dispersion correction with the Becke–Johnson damping<sup>79</sup> was used in the DFT calculations. All of the computations were performed using the Gaussian 16 program.<sup>80</sup> The donor–acceptor electron transfer coupling was computed using the generalized Mulliken–Hush approach<sup>81</sup> with TDDFT computed dipole moments and transition dipole moments. The transition dipole moments between excited states were approximated using the response functions derived from linear response TDDFT calculations, and this approximation was validated by quadratic response TDDFT computations implemented in the DAL-TON2018 program.<sup>82</sup> We benchmarked a wide range of DFT functionals and found that the donor–acceptor system of interest is best described using the pbe0 functional.

## RESULTS

**Synthesis.** Details of the synthetic procedures and characterization of 1 and 2 are given in the Supporting Information.

**Steady-State Spectroscopy.** The normalized steady-state absorption spectra of 1 and 2 in toluene are shown in Figure 3.

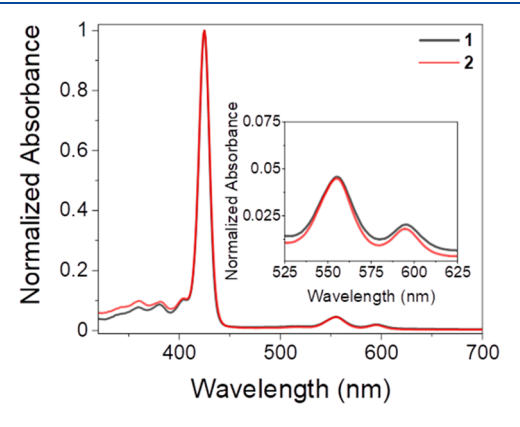


Figure 3. Normalized steady-state UV—visible absorption of  $\bf 1$  and  $\bf 2$  in toluene at 295 K. Inset expands the ZnP Q-band region of the spectra.

Both 1 and 2 have similar absorption features with the NDI vibronic progression seen at 338, 360, and 381 nm. The intensity of these features is stronger in 2 owing to the second NDI unit. The normalized absorption intensity of 2 is not exactly twice that of 1 likely because of electronic coupling due to H-aggregation between the two NDI units. The Soret band of ZnP occurs at 425 nm along with a shoulder at 404 nm. The Q(1,0) band of ZnP appears at 555 nm and the Q(0,0) band at 595 nm in both compounds. The An absorption is observed in the UV with small contributions to the spectrum between 300 and 350 nm that overlaps with the 338 and 360 nm NDI absorptions.

**Transient Absorption Spectroscopy.** Femtosecond and nanosecond transient absorption spectroscopies, fsTA and nsTA, respectively, were used to elucidate the excited-state dynamics of 1 and 2. The excited singlet state of ZnP (1\*ZnP) was populated by exciting the Soret band using 414 nm laser pulses. Experiments were carried out in toluene at 295 K under a nitrogen atmosphere. The fsTA spectra for 1 and 2 (Figure 4) have many of the same spectral features; however, the excited-state dynamics are different. Immediately after photoexcitation, the spectra show features of 1\*ZnP: namely, excited-state absorptions at 380, 459, and 1281 nm; ground-state

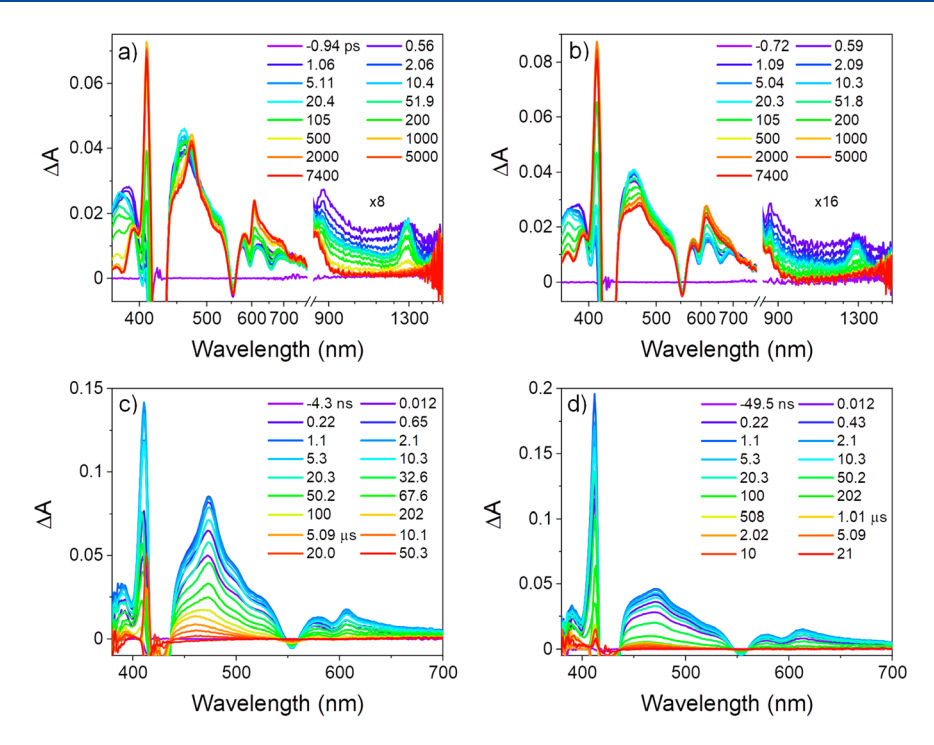
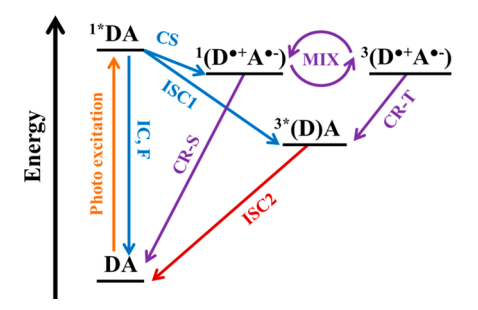


Figure 4. Transient absorption spectra at 295 K in toluene. FsTA spectra for (a) 1 and (b) 2. NsTA spectra for (c) 1 and (d) 2.

bleaching of the Soret band at 425 nm; ground-state bleaching of the Q(1,0) band at 554 nm, overlapping ground-state bleaching and stimulated emission of the Q(0,0) band at 595 nm; and stimulated emission of the Q(1,0) band at 652 nm. As the features of <sup>1</sup>\*ZnP decay, the absorption features of ZnP<sup>6+</sup> at 411 nm and NDI<sup>6-</sup> at 473 and 608 nm, as well as the ground-state bleaches of NDI at 357 and 399 nm, appear, which together are indicative of charge separation. This charge-separated species is present throughout the ~8 ns pump—probe time delay range of the fsTA experiment and is the first species observed at the start of the nsTA experiment. At these longer times, the features of <sup>3</sup>\*ZnP appear as positive absorptions at 391 and 458 nm as the SQP features decay.

The fsTA and nsTA data were subjected to global analysis with states A, B, C, and G representing the <sup>1</sup>\*ZnP, ZnP<sup>•+</sup>-An-NDI•-, or ZnP•+-An-NDI<sub>2</sub>•-, 3\*ZnP and the ground states, respectively. The evolution-associated spectra (EAS) along with kinetic fits and model populations are shown in Figures S1 and S2. The effective  $^{1*}$ ZnP decay rate constant  $k_{AB}$  is the sum of the rate constants for the processes indicated in Figure 5. The rate constant  $k_{\rm BC}$  is a composite of several processes involving the SQP including charge recombination from the singlet and triplet SQP states to the ground state ( $k_{CRS}$ ) and  $^{3*}$ ZnP ( $k_{CRT}$ ), respectively, and spin mixing of the singlet and triplet SQP states which can be kinetically modeled using an equilibrium constant  $(K_{\text{MIX}})$ . 48,49 The rate constant  $k_{\text{CG}}$ captures the decay of 3\*ZnP to the singlet ground state  $(k_{\rm ISC2})$ . A summary of the rate constants obtained from global fitting are given in Table 1.

**Magnetic Field Effects.** NsTA measurements show that the <sup>3</sup>\*ZnP yield resulting from charge recombination within the <sup>3</sup>(ZnP<sup>•+</sup>-An-NDI<sup>•-</sup>) and <sup>3</sup>(ZnP<sup>•+</sup>-An-NDI<sub>2</sub><sup>•-</sup>) SQPs is magnetic field dependent (Figure 6). The Zeeman interaction changes the energies of the  $|T_{+1}\rangle$  and  $|T_{-1}\rangle$  states of these SQPs, <sup>36</sup> which results in an observed resonance in the <sup>3</sup>\*ZnP yield at the magnetic field where  $|T_{+1}\rangle$  crosses  $|S\rangle$  (2J > 0) that



**Figure 5.** Jablonski diagram for 1 and 2. IC = internal conversion, F = fluorescence, CS = charge separation, ISC = intersystem crossing, MIX = singlet—triplet SQP spin mixing, CRS = charge recombination to singlet, and CRT = charge recombination to triplet.

Table 1. Rate Constants in Toluene at 295 K Obtained from the Transient Absorption Spectroscopy Data<sup>a</sup>

rate constant	1 (s <sup>-1</sup> )	2 (s <sup>-1</sup> )
$k_{ m AB}$	$(3.20 \pm 0.01) \times 10^9$	$(8.90 \pm 0.05) \times 10^9$
$k_{ m BC}$	$(2.71 \pm 0.05) \times 10^7$	$(2.16 \pm 0.05) \times 10^7$
$k_{CG}$	$(8.26 \pm 0.03) \times 10^4$	$(7.70 \pm 0.01) \times 10^4$

 $^ak_{\rm AB}$  values are from the fsTA data, while  $k_{\rm BC}$  and  $k_{\rm CG}$  values are from the nsTA data.

directly yields 2J (Figure 1).<sup>36,50</sup> Fitting the data to Lorentzian functions gives maxima at  $2J_1 = 210$  mT for <sup>3</sup>\*ZnP-An-NDI and  $2J_2 = 236$  mT for <sup>3</sup>\*ZnP-An-NDI<sub>2</sub> (Figure 6).

#### DISCUSSION

**Charge Transfer Dynamics.** The charge separation rate constants ( $k_{\rm CS}$ ) of 1 and 2 are obtained by subtracting the rate constant for the decay of <sup>1</sup>\*ZnP with no acceptors (4.2  $\pm$  0.1  $\times$  10<sup>8</sup> s<sup>-1</sup>)<sup>51</sup> from  $k_{\rm AB}$ , which gives (2.78  $\pm$  0.01)  $\times$  10<sup>9</sup> s<sup>-1</sup> and (8.48  $\pm$  0.05)  $\times$  10<sup>9</sup> s<sup>-1</sup> for 1 and 2, respectively, with charge separation quantum yields of 0.87 and 0.95, respectively. Given

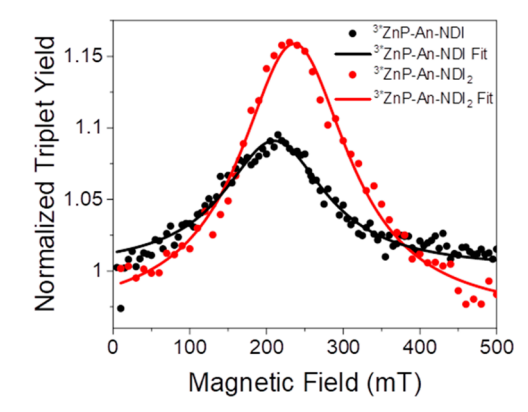


**Figure 6.** Magnetic field dependence of the normalized yield of <sup>3\*</sup>ZnP-An-NDI and <sup>3\*</sup>ZnP-An-NDI<sub>2</sub> in toluene at 295 K with associated fits.

that 2 has two NDI acceptors and 1 has one NDI acceptor, using a purely statistical basis one would expect  $k_{\rm CS}$  for 2 to be twice that of 1, whereas it is about three times as large. The free energy changes for the charge separation reactions  $^{1*}$ ZnP-An-NDI  $\rightarrow$  ZnP $^{\bullet+}$ -An-NDI $^{\bullet-}$  and  $^{1*}$ ZnP-An-NDI $_{2}$   $\rightarrow$  ZnP $^{\bullet+}$ -An-NDI $_{2}$  are  $\Delta G_{\rm CS} = -0.27$  eV and -0.36 eV, respectively, while the total nuclear reorganization energies for these same processes are  $\lambda = 0.29$  eV for 1 and  $\lambda = 0.32$  eV for 2 (see Supporting Infomation). Comparing  $\Delta G_{\rm CS}$  to  $\lambda$  shows that charge separation for both molecules occurs near the maximum of the Marcus rate vs free energy dependence, <sup>52,53</sup> which suggests that a small increase in the electronic coupling matrix element,  $V_{\rm CS}$ , for charge separation in 2 relative to 1 may be responsible for the observed  $k_{\rm CS}(2)/k_{\rm CS}(1)$  rate ratio. Using eq 1: <sup>54</sup>

$$k_{CS} = \frac{2\pi}{\hbar} |V_{CS}|^2 (4\pi \lambda_S k_B T)^{-1/2}$$

$$\sum_{m=0}^{\infty} (s^m e^{-s}/m!) e^{-(\Delta G_{CS} + \lambda_S + m\omega)^2/(4\lambda_S k_B T)}$$
(1)

where  $k_{\rm CS}$  and  $\Delta G_{\rm CS}$  are given above, the internal and solvent reorganization energies  $\lambda_i$  and  $\lambda_S$  are obtained as described in the Supporting Infomation,  $S = \lambda_i/\hbar_\omega$ , and  $\omega$  is assumed to be approximately 1500 cm<sup>-1</sup> as is typical for aromatic donors and acceptors. The values of  $V_{\rm CS}$  for 1 and 2 are 2.9 and 7.4 cm<sup>-1</sup>, respectively.

The free energies of reaction for charge recombination to the singlet ground state are  $\Delta G_{\rm CRS} = -1.79$  eV for  ${\rm ZnP}^{\bullet+}$ -An-NDI $^{\bullet-}$  and -1.70 eV for  ${\rm ZnP}^{\bullet+}$ -An-NDI $^{\bullet-}$ , while those for charge recombination to  ${}^3*{\rm ZnP}$  ( $E_{\rm T}=1.6$  eV) are  $\Delta G_{\rm CRT}=-0.19$  eV and -0.10 eV, respectively (see the Supporting Infomation). Charge recombination to the singlet ground state for both compounds falls well into the Marcus inverted region,  ${}^{55,56}$  while charge recombination to  ${}^3*{\rm ZnP}$  is in the Marcus normal region for both compounds, as is common for these reactions. Given the relative values of  $\Delta G_{\rm CRS}$  for  ${}^1({\rm ZnP}^{\bullet+}$ -An-NDI $^{\bullet-}$ ) and  ${}^1({\rm ZnP}^{\bullet+}$ -An-NDI $^{\bullet-}$ ), electron transfer theory predicts that  $k_{\rm CRS}$  for  ${}^1({\rm ZnP}^{\bullet+}$ -An-NDI $^{\bullet-}$ ) should be larger than  ${}^1({\rm ZnP}^{\bullet+}$ -An-NDI $^{\bullet-}$ ) and  ${}^3({\rm ZnP}^{\bullet+}$ -An-NDI $^{\bullet-}$ ) predict that  $k_{\rm CRT}$  for  ${}^3({\rm ZnP}^{\bullet+}$ -An-NDI $^{\bullet-}$ ) should be larger than  ${}^3({\rm ZnP}^{\bullet+}$ -An-NDI $^{\bullet-}$ ). Thus, the fact that the overall experimental charge recombination rate constant  $k_{\rm CR}$  for 1 is larger than that of 2 ( $k_{\rm BC}$  in Table 1) suggests that  $k_{\rm CRT} > k_{\rm CRS}$ .

However, one needs to be cautious because the kinetic competition between the singlet and triplet recombination pathways is also modulated by  $K_{\rm MIX}$  between the  $|{\rm S}\rangle$  and  $|{\rm T_0}\rangle$  states. This constant has been shown to vary inversely with  $2J_{\rm f}^{.57}$  however, the exact dependence and the reliance on the acceptor—acceptor coupling,  $V_{\rm AA}$ , remain unclear.

The charge recombination dynamics are well-described by a single exponential decay process in the nsTA data. This implies either that the electron hopping rate constant,  $k_{\rm hop}$ , between the two NDI units in 2 is either much larger than  $k_{\rm CRS}$  and  $k_{\rm CRT}$  or that the electron is delocalized between the two NDI units. If hopping occurs, the rate is estimated to be  $k_{hop} \gtrsim 10^{10}~{\rm s}^{-1}$  at 295 K based on the observation of hopping in a similar covalent NDI dimer using continuous-wave electron paramagnetic resonance (CW-EPR) spectroscopy. Such a rapid hopping time is well below the instrument resolution of the nanosecond transient absorption measurement ( $\sim\!0.6~{\rm ns}$ ) and is indeed on the same time scale or faster than the initial charge separation event, ensuring that electron hopping is not directly observable in this experiment. Fast hopping processes have been shown to be a source of spin decoherence in SQPs.

Electron delocalization between the acceptors can be probed directly using time-resolved femtosecond infrared (fsIR) spectroscopy. Charge delocalization is expected to result in a change in the vibrational frequencies associated with the dimeric acceptor compared to those of the single localized anion due to mode softening from differences in bond orders. The fsIR spectra for 1 and 2 in 1,4-dioxane-d<sub>8</sub> following 560 nm excitation are shown in Figures S7 and S8, respectively, and were subjected to the same kinetic analysis as the fsTA data discussed above. 1,4-Dioxane-d<sub>8</sub> was used instead of toluene for the fsIR and FTIR measurements to avoid the vibrational modes of toluene overlapping with our desired signals. Mode assignments and fitting information are given in the Supporting Infomation. The IR spectrum of <sup>1</sup>\*ZnP is weak and featureless and is replaced by strong absorptions in both compounds at 1270, 1518, 1600, and 1635 cm<sup>-1</sup>, along with bleaches of the NDI C=O stretches at frequencies above 1650 cm<sup>-1</sup>. These features appear with  $k_{AB} = (3.79 \pm 0.06) \times 10^9 \text{ s}^{-1}$  and  $(1.19 \pm 0.06) \times 10^9 \text{ s}^{-1}$  $(0.01) \times 10^{10} \text{ s}^{-1}$ , respectively, which are somewhat faster than the rate constants observed in toluene (Table 1) and then decay to a combination of ground and triplet states (Figure 7). The CR rate constants are also faster in 1,4-dioxane- $d_8$  relative to those in toluene with  $k_{\rm BC} = (1.36 \pm 0.01) \times 10^8 \, {\rm s}^{-1}$  and  $(1.05 \pm 0.01) \times 10^8 \text{ s}^{-1}$ , respectively. The difference in rate constants between 1,4-dioxane- $d_8$  and toluene is likely a

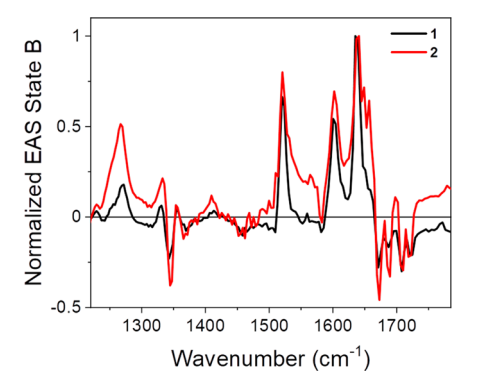


**Figure 7.** Normalized state B from the fsIR EAS for 1 and 2. Samples were prepared in 1,4-dioxane- $d_8$  and excited at 560 nm.

consequence of coordination of the Zn in the ZnP donor to an oxygen atom of 1,4-dioxane- $d_8$  resulting in ZnP being slightly easier to oxidize and thus  $\Delta G_{\rm CS}$  becoming more negative for both 1 and 2, which is a well-known phenomenon for zinc porphyrins. The corresponding fsTA spectra for 1 and 2 in 1,4-dioxane- $d_8$  are given in Figures S3–S6. A comparison of the SQP EAS (state B) of each compound shows that the spectra are nearly identical (Figure 7); this finding is consistent with our previous work on  $\pi$ -stacked acceptors. The spectral similarity indicates that at room temperature the electron is localized on a single NDI unit and that any hopping must be occurring on a time scale slower than the vibrational periods probed and thus the electron is not delocalized between the two NDI units.

Theoretical analysis supports the extent of charge localization indicated by the IR spectra. For the equilibrium geometry of the singlet charge separated state, the singly occupied molecular orbital is only partially delocalized (Figure S10) between the two NDI acceptors in 2. The computed negative charges, i.e. the Hirshfeld charge populations, are -0.77 and -0.12 for the two NDI acceptors. Stretching the structure slightly along the two NDI bending modes at an energy cost of about 300 cm<sup>-1</sup> leads to essentially full charge localization. The computed singlet charge separation couplings (Tables S1-S4) agree within factors of 3-4 with the values derived from experiment using eq 1, in addition to predicting that  $V_{CS}$  (2) >  $V_{CS}$  (1). Furthermore, the computed donor acceptor charge recombination electronic couplings,  $V_{\rm CR}$ , (Tables S5-S8) are comparable in magnitude irrespective of whether there are one or two NDI acceptors.

Delocalization of the charge must be supported by an appropriate acceptor-acceptor coupling interaction,  $V_{\rm AA}$ . Since thermal fluctuations tend to localize charges through modulations of the local electronic and environmental symmetries, for coherence to be maintained  $V_{\rm AA}$  must be larger than  $k_{\rm B}T$ . At the same time, the coupling cannot be so strong that the reaction free energy is dramatically changed, and the symmetric combination of acceptor orbitals is overly stabilized. Here, the splitting between the reduction potentials,  $2V_{\rm AA}=90~{\rm meV},^{40}$  shows that  $V_{\rm AA}$  is less than two times  $k_{\rm B}T$  at room temperature. While this coupling strength satisfies the first criterion, it may not be is sufficiently large to overcome the influence of thermal fluctuations that will tend to produce charge localization on a single acceptor species.

As we have discussed earlier,  $^{10,11}$  coherent charge recombination from a delocalized acceptor would result in a factor of  $\sqrt{2}$  higher DA coupling compared to the case of localization on a single acceptor, and thus a factor of 2 enhancement in the recombination rate, according to eq 1. However, the observed total recombination rate to the singlet ground and lowest triplet states in 2 is actually slower than in 1. The free energies for recombination discussed above are different enough that eq 1 adequately predicts the behavior of the rates in the absence of coherent delocalization on the two acceptors. Moreover, the similarity of the fsIR spectra strongly suggests that the charge has localized prior to recombination; since charge hopping between the two NDIs is incoherent, the electron density is always restricted to one NDI unit on the vibrational time scale.

**Spin Dynamics.** Focusing on the triplet state, the  $^{3*}$ ZnP quantum yield in the absence of the NDI acceptors that results from spin-orbit-induced intersystem crossing is 0.9. Assuming internal conversion is negligible,  $\phi_{ISC1} = \phi_T (1 - \phi_{CS})$ , thus  $\phi_{ISC1} = 0.07 \pm 0.02$  for 1 and 0.03  $\pm$  0.02 for 2. In

contrast, the observed  $^{3*}$ ZnP yields for 1 and 2 determined from the nsTA data and the extinction coefficients of closely related Zn porphyrins,  $^{62,63}$  are  $0.95 \pm 0.02$  and  $0.60 \pm 0.02$ , respectively (see Supporting Infomation). This shows that the majority of the observed  $^{3*}$ ZnP is derived from SQP recombination ( $k_{\text{CRT}}$ , Figure 5) and only a small portion of  $^{3*}$ ZnP comes from the intersystem crossing mechanism.

The spin–spin exchange coupling 2*J* of an SQP is related to the electronic coupling matrix elements between the SQP and nearby electronic states. <sup>64–67</sup> Given that the principal states coupled to the SQP are the <sup>1</sup>\*ZnP-An-NDI (or NDI<sub>2</sub>) excited states that precede charge separation and the ZnP-An-NDI (or NDI<sub>2</sub>) ground and <sup>3</sup>\*ZnP-An-NDI (or NDI<sub>2</sub>) states that result from charge recombination, then

$$2J = \frac{V_{CRT}^2}{\Delta G_{CRT} + \lambda} - \frac{V_{CRS}^2}{\Delta G_{CRS} + \lambda} - \frac{V_{CS}^2}{\Delta G_{CS} + \lambda}$$
(2)

where the indicated matrix elements  $V_{CS}$ ,  $V_{CRS}$ , and  $V_{CRT}$  couple the singlet and triplet SQP states to  $^{1*}$ ZnP, the singlet ground state, and  $^{3*}$ ZnP, respectively,  $\Delta G_{CS}$ ,  $\Delta G_{CRS}$ ,  $\Delta G_{CRT}$ , and  $\lambda$  were defined and given earlier, and it is assumed that  $\lambda$  is the same for each charge transfer process. Given that the donor and acceptor both involve relatively large  $\pi$  systems, we also assume that  $V_{CRS}^{2} = V_{CRT}^{2}$  for each SQP, so that eq 2 can be simplified to

$$2J = V_{CR}^2 \left[ \frac{1}{\Delta G_{CRT} + \lambda} - \frac{1}{\Delta G_{CRS} + \lambda} \right] - \frac{V_{CS}^2}{\Delta G_{CS} + \lambda}$$
(3)

Using  $V_{CS}$  for 1 and 2 obtained from our data and eq 1, the corresponding experimental values of  $2J_1$  and  $2J_2$ , as well as  $\Delta G_{CS}$ ,  $\Delta G_{CRS}$ ,  $\Delta G_{CRT}$ , and  $\lambda$  for 1 and 2 given above, eq 3 yields  $V_{CR}(1) = 15 \text{ cm}^{-1}$  and  $V_{CR}(2) = 10 \text{ cm}^{-1}$ , which is consistent with the observation that  $k_{CR}(1) > k_{CR}(2)$  (Table 1) and the computed values of  $V_{CR}$  (Tables S5-S8). As noted above, theory predicts that CR proceeding by a coherent superexchange mechanism comprising two equivalent pathways from a delocalized acceptor would give  $V_{CR}(2)$  =  $\sqrt{2V_{CR}(1)}$ . 40,68-70 On the basis of the free energy, reorganization energy, and  $V_{CS}$  estimates described above, we found  $V_{CR}(2) = 0.67 V_{CR}(1)$  meaning CR for 2 is not an electronically coherent process. Nevertheless, our studies of related multiacceptor systems show that incoherent electron hopping between nearly equivalent sites occurs with  $k_{hop} \gtrsim$  $10^{10} \, \mathrm{s}^{-1}$  at 295 K.<sup>41</sup>

Although CR is electronically incoherent, the observed magnetic field effects are consistent with CR for both 1 and 2 being spin coherent. The resonance line shapes in the magnetic field effect data (Figure 6) for 1 and 2 provide information on hyperfine interactions and spin decoherence and relaxation effects.<sup>71</sup> Given the relatively small *g*-factor difference between the radicals that comprise each SQP, the hyperfine interaction primarily determines  $|S\rangle \leftrightarrow |T_{+1}\rangle$  mixing. However, the mean hyperfine fields of 1 and 2 are only 1.46 and 1.38 mT, respectively, using models<sup>57</sup> that employ previously reported values for the radicals. 41,72 Using these mean hyperfine fields and a previously reported model (see Supporting Infomation),73 the resulting rate constants for hyperfine mixing of  $^{1,3}(ZnP^{\bullet+}-An-NDI^{\bullet-})$  and  $^{1,3}(ZnP^{\bullet+}-An-NDI_2^{\bullet-})$  are  $4.1 \times 10^6$  $\rm s^{-1}$  and 3.9  $\times$  10<sup>6</sup>  $\rm s^{-1}$ , respectively. Given the similarities of the two estimated hyperfine contributions, these interactions do not adequately account for the differences in line shape and width of the field dependent 3\*ZnP yield data for 1 and 2 (Figure 6). The large full-width at half-maximum values of 163 mT for 1 and 173 mT for 2 indicate that spin decoherence contributes to line broadening to a larger degree in 2 relative to 1.<sup>71</sup> Additionally, the asymmetric baseline in 2, specifically the normalized triplet yield dropping below 1 at high magnetic fields, also supports the important role of decoherence effects.<sup>71</sup> Interestingly, since the D-C-A and D-C-A<sub>2</sub> systems studied in our previous investigation had 2J values that were relatively small, both hyperfine interactions and relaxation effects gave rise to differences in both the shape and peak position of the 2J resonance. Compounds 1 and 2 provide an advantage over that earlier study in that they illustrate the fact that rapid electron hopping between the two NDI sites in 2 affects spin decoherence in a regime where the relative hyperfine interactions are not a factor.

#### CONCLUSIONS

Following photoexcitation of 1 and 2 in toluene at 295 K, femtosecond transient absorption spectroscopy shows that the ET rate constant for 2 is about three times larger than that of 1, which can be accounted for by the statistical nature of incoherent ET as well as a small change in free energy of reaction. In contrast, the rate constant for CR of 1 is about 25% faster than that of 2. Using femtosecond transient infrared spectroscopy and theoretical analysis, we find that the electron on NDI<sub>2</sub> in 2 localizes onto one of the two NDIs prior to CR, thus precluding electronically coherent CR from NDI<sub>2</sub>. Conversely, CR in both 1 and 2 is spin coherent as indicated by the observation of a resonance in the <sup>3</sup>\*ZnP yield following CR as a function of applied magnetic field, giving spin-spin exchange interaction energies of 2J = 210 and 236 mT, respectively, where the line width of the resonance for 2 is greater than 1. These data show that while CR is a spincoherent process, incoherent hopping of the electron between the two NDIs in 2, consistent with the lack of delocalization noted above, results in greater spin decoherence in 2 relative to

Designing D-A2 systems that achieve coherent electron transfer at room temperature poses a particular challenge due to the localizing nature of thermal fluctuations. The requirements of  $k_{\rm B}T\ll 2V_{\rm AA}$  and small  $V_{\rm AA}$  necessarily restrict the operable temperature range. While lowering the temperature has been shown to enable delocalization, increasing  $V_{\rm AA}$  will only reduce the probability for coherent electron transfer, because of the free energy effects discussed above. A balance of these factors may exist, where a carefully tuned  $V_{\mathrm{AA}}$  would enable this process. The acceptor-acceptor coupling must be modulated in such a way that the  $V_{\mathrm{DA}}$  between the donor and each acceptor remains approximately equal. This constraint rules out the use of asymmetric spacers and typical slipstacking strategies, which would bias one acceptor in favor of another. Alternatively, modification of the solubilizing tails or side groups could splay the acceptors slightly, lessening their electronic coupling. The use of a different linker group, where the acceptors are noncofacially oriented, could also be used to greater effect, although this would also impart greater flexibility and disorder, which could also disrupt the required degeneracy. Overall, much work needs to be done to identify molecules that meet all of these requirements.

## ASSOCIATED CONTENT

# Supporting Information

The Supporting Information is available free of charge at https://pubs.acs.org/doi/10.1021/acs.jpca.0c10471.

Synthesis and characterization of 1 and 2, additional transient optical absorption data and kinetic analysis, free energy of reaction and reorganization energy calculational details, additional magnetic field effect data, and density functional theory computations (PDF)

## AUTHOR INFORMATION

## **Corresponding Authors**

Michael R. Wasielewski — Department of Chemistry and Institute for Sustainability and Energy at Northwestern, Northwestern University, Evanston, Illinois 60208-3113, United States; Occid.org/0000-0003-2920-5440; Email: m-wasielewski@northwestern.edu

Ryan M. Young — Department of Chemistry and Institute for Sustainability and Energy at Northwestern, Northwestern University, Evanston, Illinois 60208-3113, United States; orcid.org/0000-0002-5108-0261; Email: ryan.young@northwestern.edu

David N. Beratan — Department of Chemistry and Departments of Biochemistry and Physics, Duke University, Durham, North Carolina 27708, United States;
ocid.org/0000-0003-4758-8676;

Email: david.beratan@duke.edu

#### Authors

Laura Bancroft — Department of Chemistry and Institute for Sustainability and Energy at Northwestern, Northwestern University, Evanston, Illinois 60208-3113, United States; orcid.org/0000-0002-4312-9758

Jinyuan Zhang — Department of Chemistry and Institute for Sustainability and Energy at Northwestern, Northwestern University, Evanston, Illinois 60208-3113, United States

Samantha M. Harvey – Department of Chemistry and Institute for Sustainability and Energy at Northwestern, Northwestern University, Evanston, Illinois 60208-3113, United States

Matthew D. Krzyaniak – Department of Chemistry and Institute for Sustainability and Energy at Northwestern, Northwestern University, Evanston, Illinois 60208-3113, United States; orcid.org/0000-0002-8761-7323

Peng Zhang – Department of Chemistry, Duke University, Durham, North Carolina 27708, United States

Richard D. Schaller – Department of Chemistry and Institute for Sustainability and Energy at Northwestern, Northwestern University, Evanston, Illinois 60208-3113, United States; Center for Nanoscale Materials, Argonne National Laboratory, Lemont, Illinois 60439, United States

Complete contact information is available at: https://pubs.acs.org/10.1021/acs.jpca.0c10471

#### **Notes**

The authors declare no competing financial interest.

## ACKNOWLEDGMENTS

We thank Dr. Brian T. Phelan for the preliminary kinetic studies and helpful broader discussions of these molecules. This work was supported by the National Science Foundation under Award CHE-1925690 (M.R.W., D.N.B., P.Z.). S.M.H. is

supported by the National Science Foundation Graduate Research Fellowship Program under Grant No. DGE-1842165. This work was performed, in part, at the Center for Nanoscale Materials, a U.S. Department of Energy Office of Science User Facility, and supported by the U.S. Department of Energy, Office of Science, under Contract No. DE-AC02-06CH11357 (R.D.S.).

## REFERENCES

- (1) Krüger, H. W.; Michel-Beyerle, M. E.; Seidlitz, H. The influence of electron hopping on the recombination dynamics of radical ion pairs in liquid solution. *Chem. Phys. Lett.* **1982**, *87*, 79–82.
- (2) Michel-Beyerle, M. E.; Krüger, H. W.; Haberkorn, R.; Seidlitz, H. Nanosecond time-resolved magnetic field effect on radical recombination in solution. *Chem. Phys.* **1979**, *42*, 441–447.
- (3) Haberkorn, R.; Michel-Beyerle, M. E.; Marcus, R. A. On spin-exchange and electron-transfer rates in bacterial photosynthesis. *Proc. Natl. Acad. Sci. U. S. A.* 1979, 76, 4185–4188.
- (4) Liu, Y.; Flood, A. H.; Moskowitz, R. M.; Stoddart, J. F. Versatile self-complexing compounds based on covalently linked donor—acceptor cyclophanes. *Chem. Eur. J.* **2005**, *11*, 369–385.
- (5) Phelan, B. T.; Zhang, J.; Huang, G.-J.; Wu, Y.-L.; Zarea, M.; Young, R. M.; Wasielewski, M. R. Quantum coherence enhances electron transfer rates to two equivalent electron acceptors. *J. Am. Chem. Soc.* **2019**, *141*, 12236–12239.
- (6) Werner, U.; Sakaguchi, Y.; Hayashi, H.; Nohya, G.; Yoneshima, R.; Nakajima, S.; Osuka, A. Magnetic field effects in the radical ion pair recombination of fixed-distance triads consisting of porphyrins and an electron acceptor. *J. Phys. Chem.* **1995**, *99*, 13930–13937.
- (7) Wu, Y.; Zhou, J.; Nelson, J. N.; Young, R. M.; Krzyaniak, M. D.; Wasielewski, M. R. Covalent radical pairs as spin qubits: Influence of rapid electron motion between two equivalent sites on spin coherence. *J. Am. Chem. Soc.* **2018**, *140*, 13011–13021.
- (8) McConnell, H. M. Electron densities in semiquinones by paramagnetic resonance. *J. Chem. Phys.* **1956**, *24*, 632–632.
- (9) McConnell, H. M. Indirect hyperfine interactions in the paramagnetic resonance spectra of aromatic free radicals. *J. Chem. Phys.* **1956**, *24*, 764–766.
- (10) Phelan, B. T.; Zhang, J.; Huang, G.-J.; Wu, Y.-L.; Zarea, M.; Young, R. M.; Wasielewski, M. R. Quantum coherence enhances electron transfer rates to two equivalent electron acceptors. *J. Am. Chem. Soc.* **2019**, *141*, 12236–12239.
- (11) Phelan, B. T.; Schultz, J. D.; Zhang, J.; Huang, G.-J.; Young, R. M.; Wasielewski, M. R. Quantum coherence in ultrafast photo-driven charge separation. *Faraday Discuss.* **2019**, *216*, 319–338.
- (12) Daviso, E.; Alia, A.; Prakash, S.; Diller, A.; Gast, P.; Lugtenburg, J.; Matysik, J.; Jeschke, G. Electron–nuclear spin dynamics in a bacterial photosynthetic reaction center. *J. Phys. Chem. C* **2009**, *113*, 10269–10278.
- (13) Hoff, A. J.; Rademaker, H.; Van Grondelle, R.; Duysens, L. N. M. On the magnetic field dependence of the yield of the triplet state in reaction centers of photosynthetic bacteria. *Biochim. Biophys. Acta, Bioenerg.* **1977**, 460, 547–554.
- (14) Wasielewski, M. R. Self-assembly strategies for integrating light harvesting and charge separation in artificial photosynthetic systems. *Acc. Chem. Res.* **2009**, *42*, 1910–1921.
- (15) Rudolf, M.; Kirner, S. V.; Guldi, D. M. A multicomponent molecular approach to artificial photosynthesis the role of fullerenes and endohedral metallofullerenes. *Chem. Soc. Rev.* **2016**, *45*, 612–630.
- (16) Biskup, T.; Schleicher, E.; Okafuji, A.; Link, G.; Hitomi, K.; Getzoff, E. D.; Weber, S. Direct observation of a photoinduced radical pair in a cryptochrome blue-light photoreceptor. *Angew. Chem., Int. Ed.* **2009**, *48*, 404–407.
- (17) Hiscock, H. G.; Worster, S.; Kattnig, D. R.; Steers, C.; Jin, Y.; Manolopoulos, D. E.; Mouritsen, H.; Hore, P. J. The quantum needle of the avian magnetic compass. *Proc. Natl. Acad. Sci. U. S. A.* **2016**, 113, 4634–4639.

- (18) Kelber, J. B.; Panjwani, N. A.; Wu, D.; Gómez-Bombarelli, R.; Lovett, B. W.; Morton, J. J. L.; Anderson, H. L. Synthesis and investigation of donor—porphyrin—acceptor triads with long-lived photo-induced charge-separate states. *Chem. Sci.* **2015**, *6*, 6468—6481.
- (19) Krzyaniak, M. D.; Kobr, L.; Rugg, B. K.; Phelan, B. T.; Margulies, E. A.; Nelson, J. N.; Young, R. M.; Wasielewski, M. R. Fast photo-driven electron spin coherence transfer: The effect of electron-nuclear hyperfine coupling on coherence dephasing. *J. Mater. Chem. C* **2015**, *3*, 7962–7967.
- (20) Nelson, J. N.; Krzyaniak, M. D.; Horwitz, N. E.; Rugg, B. K.; Phelan, B. T.; Wasielewski, M. R. Zero quantum coherence in a series of covalent spin-correlated radical pairs. *J. Phys. Chem. A* **2017**, *121*, 2241–2252.
- (21) Nelson, J. N.; Zhang, J.; Zhou, J.; Rugg, B. K.; Krzyaniak, M. D.; Wasielewski, M. R. Cnot gate operation on a photogenerated molecular electron spin-qubit pair. *J. Chem. Phys.* **2020**, *152*, 014503.
- (22) Rugg, B. K.; Krzyaniak, M. D.; Phelan, B. T.; Ratner, M. A.; Young, R. M.; Wasielewski, M. R. Photodriven quantum teleportation of an electron spin state in a covalent donor-acceptor-radical system. *Nat. Chem.* **2019**, *11*, 981–986.
- (23) Norris, J. R.; Uphaus, R. A.; Crespi, H. L.; Katz, J. J. Electron spin resonance of chlorophyll and the origin of signal I in photosynthesis. *Proc. Natl. Acad. Sci. U. S. A.* 1971, 68, 625–628.
- (24) Polizzi, N. F.; Jiang, T.; Beratan, D. N.; Therien, M. J. Engineering opposite electronic polarization of singlet and triplet states increases the yield of high-energy photoproducts. *Proc. Natl. Acad. Sci. U. S. A.* **2019**, *116*, 14465–14470.
- (25) DiVincenzo, D. P. The physical implementation of quantum computation. *Fortschr. Phys.* **2000**, *48*, 771–783.
- (26) Schulten, K.; Wolynes, P. G. Semi-classical description of electron-spin motion in radicals including effect of electron hopping. *J. Chem. Phys.* **1978**, *68*, 3292–3297.
- (27) Knapp, E. W.; Schulten, K. Magnetic field effect on the hyperfine-induced electron spin motion in radicals undergoing diamagnetic-paramagnetic exchange. *J. Chem. Phys.* **1979**, *71*, 1878–1883.
- (28) Schulten, K. The effect of intramolecular paramagnetic-diamagnetic exchange on the magnetic field effect of radical pair recombination. *J. Chem. Phys.* **1985**, 82, 1312–16.
- (29) Michel-Beyerle, M. E.; Krueger, H. W.; Haberkorn, R.; Seidlitz, H. Nanosecond time-resolved magnetic field effect on radical recombination in solution. *Chem. Phys.* **1979**, *42*, 441–7.
- (30) Haberkorn, R.; Michel-Beyerle, M. E.; Marcus, R. On spin-exchange and electron-transfer rates in bacterial photosynthesis. *Proc. Natl. Acad. Sci. U. S. A.* **1979**, *76*, 4185–4188.
- (31) Krueger, H. W.; Michel-Beyerle, M. E.; Seidlitz, H. The influence of electron hopping on the recombination dynamics of radical ion pairs in liquid solution. *Chem. Phys. Lett.* **1982**, *87*, 79–82.
- (32) Krueger, H. W.; Michel-Beyerle, M. E.; Knapp, E. W. Electron hopping and magnetic field dependent spin dynamics of radical ions in solution. *Chem. Phys.* **1983**, *74*, 205–216.
- (33) Werner, U.; Sakaguchi, Y.; Hayashi, H.; Nohya, G.; Yoneshima, R.; Nakajima, S.; Osuka, A. Magnetic field effects in the radical ion pair recombination of fixed-distance triads consisting of porphyrins and an electron acceptor. *J. Phys. Chem.* **1995**, *99*, 13930–13937.
- (34) Petrov, N. K.; Alfimov, M. V.; Budyka, M. F.; Gavrishova, T. N.; Staerk, H. Intramolecular electron hopping in double carbazole molecules studied by the fluorescence-detected magnetic field effect. *J. Phys. Chem. A* **1999**, *103*, 9601–9604.
- (35) Closs, G. L.; Forbes, M. D. E.; Norris, J. R. Spin-polarized electron-paramagnetic resonance-spectra of radical pairs in micelles observation of electron spin-spin interactions. *J. Phys. Chem.* **1987**, *91*, 3592–3599.
- (36) Steiner, U. E.; Ulrich, T. Magnetic field effects in chemical kinetics and related phenomena. *Chem. Rev.* **1989**, *89*, 51–147.
- (37) Norris, J. R.; Morris, A. L.; Thurnauer, M. C.; Tang, J. A general model of electron spin polarization arising from the interactions within radical pairs. *J. Chem. Phys.* **1990**, 92, 4239–4249.

- (38) Till, U.; Hore, P. J. Radical pair kinetics in a magnetic field. *Mol. Phys.* 1997, 90, 289–296.
- (39) Tang, J.; Norris, J. R. Multiple-quantum EPR coherence in a spin-correlated radical pair system. *Chem. Phys. Lett.* **1995**, 233, 192–200
- (40) Phelan, B. T.; Schultz, J. D.; Zhang, J.; Huang, G.-J.; Young, R. M.; Wasielewski, M. R. Quantum coherence in ultrafast photo-driven charge separation. *Faraday Discuss.* **2019**, *216*, 319–338.
- (41) Wu, Y.; Nalluri, S. K. M.; Young, R. M.; Krzyaniak, M. D.; Margulies, E. A.; Stoddart, J. F.; Wasielewski, M. R. Charge and spin transport in an organic molecular square. *Angew. Chem., Int. Ed.* **2015**, 54, 11971–11977.
- (42) Weiss, E. A.; Tauber, M. J.; Ratner, M. A.; Wasielewski, M. R. Electron spin dynamics as a probe of molecular dynamics: Temperature-dependent magnetic field effects on charge recombination within a covalent radical ion pair. J. Am. Chem. Soc. 2005, 127, 6052–6061
- (43) Cao, H.; Fujiwara, Y.; Haino, T.; Fukazawa, Y.; Tung, C.-H.; Tanimoto, Y. Magnetic field effects on intramolecular exciplex fluorescence of chain-linked phenanthrene and N,N-dimethylaniline: Influence of chain length, solvent, and temperature. *Bull. Chem. Soc. Jpn.* **1996**, *69*, 2801–2813.
- (44) Walters, V. A.; de Paula, J. C.; Jackson, B.; Nutaitis, C.; Hall, K.; Lind, J.; Cardozo, K.; Chandran, K.; Raible, D.; Phillips, C. M. Electronic structure of triplet states of zinc(II) tetraphenylporphyrins. *J. Phys. Chem.* **1995**, *99*, 1166–1171.
- (4S) Basel, B. S.; Zirzlmeier, J.; Hetzer, C.; Reddy, S. R.; Phelan, B. T.; Krzyaniak, M. D.; Volland, M. K.; Coto, P. B.; Young, R. M.; Clark, T.; Thoss, M.; et al. Evidence for charge-transfer mediation in the primary events of singlet fission in a weakly coupled pentacene dimer. *Chem.* **2018**, *4*, 1092–1111.
- (46) Michl, J. In *Handbook of Photochemistry*, 3rd ed.; Montalti, M., Credi, A., Prodi, L., Gandolfi, M. T., Eds.; CRC Press, Taylor & Francis: 2006; pp 1–48.
- (47) Jones, R. N. The ultraviolet absorption spectra of anthracene derivatives. *Chem. Rev.* **1947**, *41*, 353–371.
- (48) Miura, T.; Scott, A. M.; Wasielewski, M. R. Electron spin dynamics as a controlling factor for spin-selective charge recombination in donor-bridge-acceptor molecules. *J. Phys. Chem. C* **2010**, *114*, 20370–20379.
- (49) Scott, A. M.; Miura, T.; Ricks, A. B.; Dance, Z. E. X.; Giacobbe, E. M.; Colvin, M. T.; Wasielewski, M. R. Spin-selective charge transport pathways through p-oligophenylene-linked donor-bridge-acceptor molecules. *J. Am. Chem. Soc.* **2009**, *131*, 17655–17666.
- (50) Anderson, P. W. Theory of Magnetic Exchange Interactions: Exchange in Insulators and Semiconductors. *Solid State Phys.* **1963**, 14, 99–214.
- (51) Thamyongkit, P.; Speckbacher, M.; Diers, J. R.; Kee, H. L.; Kirmaier, C.; Holten, D.; Bocian, D. F.; Lindsey, J. S. Swallowtail porphyrins: Synthesis, characterization and incorporation into porphyrin dyads. *J. Org. Chem.* **2004**, *69*, 3700–3710.
- (52) Marcus, R. A. On the theory of oxidation-reduction reactions involving electron transfer. I. J. Chem. Phys. 1956, 24, 966–978.
- (53) Marcus, R. A. Theory of electron-transfer reactions. VI. Unified treatment for homogeneous and electrode reactions. *J. Chem. Phys.* **1965**, 43, 679–701.
- (54) Closs, G. L.; Miller, J. R. Intramolecular long-distance electron transfer in organic molecules. *Science* **1988**, 240, 440–447.
- (55) Marcus, R. A. Chemical and electrochemical electron-transfer theory. *Annu. Rev. Phys. Chem.* **1964**, *15*, 155–196.
- (56) Marcus, R. A.; Sutin, N. Electron transfers in chemistry and biology. *Biochim. Biophys. Acta, Rev. Bioenerg.* 1985, 811, 265-322.
- (57) Klein, J. H.; Schmidt, D.; Steiner, U. E.; Lambert, C. Complete monitoring of coherent and incoherent spin flip domains in the recombination of charge-separated states of donor-iridium complex-acceptor triads. *J. Am. Chem. Soc.* **2015**, *137*, 11011–11021.
- (58) Denden, Z.; Ezzayani, K.; Saint-Aman, E.; Loiseau, F.; Najmudin, S.; Bonifácio, C.; Daran, J.-C.; Nasri, H. Insights on the uv/vis, fluorescence, and cyclic voltammetry properties and the

- molecular structures of ZnII tetraphenylporphyrin complexes with pseudohalide axial azido, cyanato-N, thiocyanato-N, and cyanido ligands. *Eur. J. Inorg. Chem.* **2015**, 2015, 2596–2610.
- (59) Hartnett, P. E.; Mauck, C. M.; Harris, M. A.; Young, R. M.; Wu, Y.-L.; Marks, T. J.; Wasielewski, M. R. Influence of anion delocalization on electron transfer in a covalent porphyrin donor-perylenediimide dimer acceptor system. *J. Am. Chem. Soc.* **2017**, *139*, 749–756.
- (60) Mauck, C. M.; Young, R. M.; Wasielewski, M. R. Characterization of excimer relaxation via femtosecond shortwave- and midinfrared spectroscopy. *J. Phys. Chem. A* **2017**, *121*, 784–792.
- (61) Alzola, J. M.; Powers-Riggs, N. E.; La Porte, N. T.; Young, R. M.; Marks, T. J.; Wasielewski, M. R. Photoinduced electron transfer from zinc meso-tetraphenylporphyrin to a one-dimensional perylene-diimide aggregate: Probing anion delocalization effects. *J. Porphyrins Phthalocyanines* **2020**, 24, 143–152.
- (62) Kikuchi, K.; Kurabayashi, Y.; Kokubun, H.; Kaizu, Y.; Kobayashi, H. Triplet yields of some tetraphenylporphyrins and octaethylporphyrins. *J. Photochem. Photobiol.*, A 1988, 45, 261–263.
- (63) Hurley, J. K.; Sinai, N.; Linschitz, H. Actinometry in monochromatic flash photolysis: The extinction coefficient of triplet benzophenone and quantum yield of triplet zinc tetraphenyl porphyrin. *Photochem. Photobiol.* **1983**, 38, 9–14.
- (64) Anderson, P. W. New approach to the theory of superexchange interactions. *Phys. Rev.* **1959**, *115*, 2–13.
- (65) Kobori, Y.; Sekiguchi, S.; Akiyama, K.; Tero-Kubota, S. Chemically induced dynamic electron polarization study on the mechanism of exchange interaction in radical ion pairs generated by photoinduced electron transfer reactions. *J. Phys. Chem. A* **1999**, *103*, 5416–5424.
- (66) Kramers, H. A. The interaction of magnetogenic atoms in paramagnetic crystals. *Physica* **1934**, *1*, 182–192.
- (67) Weiss, E. A.; Ratner, M. A.; Wasielewski, M. R. Direct measurement of singlet-triplet splitting within rodlike photogenerated radical ion pairs using magnetic field effects: Estimation of the electronic coupling for charge recombination. *J. Phys. Chem. A* **2003**, 107, 3639–3647.
- (68) Leggett, A. J.; Chakravarty, S.; Dorsey, A. T.; Fisher, M. P. A.; Garg, A.; Zwerger, W. Dynamics of the dissipative two-state system. *Rev. Mod. Phys.* **1987**, *59*, 1.
- (69) Nitzan, A. Chemical Dynamics in Condensed Phases: Relaxation, Transfer, and Reactions in Condensed Molecular Systems; Oxford University Press: New York, 2006.
- (70) Zarea, M.; Ratner, M. A.; Wasielewski, M. R. Electron transfer in a two-level system within a cole-davidson vitreous bath. *J. Chem. Phys.* **2014**, *140*, 024110.
- (71) Steiner, U. E.; Schäfer, J.; Lukzen, N. N.; Lambert, C. Jresonance line shape of magnetic field-affected reaction yield spectrum from charge recombination in a linked donor—acceptor dyad. J. Phys. Chem. C 2018, 122, 11701–11708.
- (72) Fajer, J.; Borg, D.; Forman, A.; Adker, A.; Varadi, V. Cation radicals of tetraalkylprophyrins. *J. Am. Chem. Soc.* **1974**, *96*, 1238–1239.
- (73) Batchelor, S.; Kay, C.; McLauchlan, K.; Shkrob, I. Timeresolved and modulation methods in the study of the effects of magnetic fields on the yields of free-radical reactions. *J. Phys. Chem.* **1993**, *97*, 13250–13258.
- (74) Young, R. M.; Dyar, S. M.; Barnes, J. C.; Juríček, M.; Stoddart, J. F.; Co, D. T.; Wasielewski, M. R. Ultrafast conformational dynamics of electron transfer in exbox<sup>4+</sup>⊂perylene. *J. Phys. Chem. A* **2013**, *117*, 12438−12448.
- (75) Mauck, C. M.; Young, R. M.; Wasielewski, M. R. Characterization of excimer relaxation via femtosecond shortwave- and midinfrared spectroscopy. *J. Phys. Chem. A* **2017**, *121*, 784–792.
- (76) Chen, M.; Krzyaniak, M. D.; Nelson, J. N.; Bae, Y. J.; Harvey, S. M.; Schaller, R. D.; Young, R. M.; Wasielewski, M. R. Quintet-triplet mixing determines the fate of the multiexciton state produced by singlet fission in a terrylenediimide dimer at room temperature. *Proc. Natl. Acad. Sci. U. S. A.* **2019**, *116*, 8178–8183.

- (77) Weigend, F.; Ahlrichs, R. Balanced basis sets of split valence, triple zeta valence and quadruple zeta valence quality for H to Rn: Design and assessment of accuracy. *Phys. Chem. Chem. Phys.* **2005**, *7*, 3297–3305.
- (78) Zheng, J. J.; Xu, X. F.; Truhlar, D. G. Minimally augmented Karlsruhe basis sets. *Theor. Chem. Acc.* **2011**, *128*, 295–305.
- (79) Grimme, S.; Ehrlich, S.; Goerigk, L. Effect of the damping function in dispersion corrected density functional theory. *J. Comput. Chem.* **2011**, 32, 1456–1465.
- (80) Frisch, M. J.; Trucks, G. W.; Schlegel, H. B.; Scuseria, G. E.; Robb, M. A.; Cheeseman, J. R.; Scalmani, G.; Barone, V.; Petersson, G. A.; Nakatsuji, H.; et al. *Gaussian 16*, Rev. A.03; Gaussian, Inc.: Wallingford, CT, 2016.
- (81) Cave, R. J.; Newton, M. D. Generalization of the mulliken-hush treatment for the calculation of electron transfer matrix elements. *Chem. Phys. Lett.* **1996**, 249, 15–19.
- (82) Aidas, K.; Angeli, C.; Bak, K. L.; Bakken, V.; Bast, R.; Boman, L.; Christiansen, O.; Cimiraglia, R.; Coriani, S.; Dahle, P.; et al. The dalton quantum chemistry program system. *Wiley Interdiscip. Rev.: Comput. Mol. Sci.* **2014**, *4*, 269–284.